A&A 439, 75–84 (2005)
DOI: 10.1051/0004-6361:20052643

Astronomy & Astrophysics

Molecular gas and continuum emission in 3C 48: evidence for two merger nuclei?

M. Krips[1], A. Eckart[1], R. Neri[2], J. Zuther[1], D. Downes[2], and J. Scharwächter[1]

[1] I. Physikalisches Institut, Universität zu Köln, Zülpicher Str. 77, 50937 Köln, Germany
e-mail: krips@ph1.uni-koeln.de
[2] Institut de Radio Astronomie Millimétrique, 300 rue de la Piscine, 38406 Saint Martin d'Hères, France

Received 5 January 2005 / Accepted 3 May 2005

Abstract. We present new interferometer observations of the CO(1–0) line and mm continuum emission from 3C 48 – one of the nearest examples of a merger activating a quasar. Our new CO data show that most of the CO is not in a disk around the quasar 3C 48, but rather in a second nucleus associated with the source 3C 48A ~ 1″ to the north-east, recently studied in the near-IR by Zuther et al. (2004). This main CO source has a strong velocity gradient (140 km s^{-1} over about 1″). Our new data also show a second, weaker CO source at the QSO itself. At 1.2 mm, the continuum emission is elongated in the direction of the radio jet and towards 3C 48A. We model the 1.2 mm continuum with three different sources in 3C 48 – the 3C 48 QSO, the 3C 48 jet, and the second nucleus 3C 48A. We suggest that the unusually bright and extended nature of the jet may be due to its interaction with the second merger nucleus 3C 48A.

Key words. galaxies: active – galaxies: kinematics and dynamics – galaxies: interaction – quasars: individual: 3C 48

1. Introduction

Galaxy mergers are regarded as part of the chain of events that can lead to the activation or re-ignition of quasars. A prime example of this phenomenon is the radio source 3C 48, one of the first quasars to be optically identified (Matthews et al. 1961). The source is known to be surrounded by an unusually large and bright host galaxy with a young stellar population (Kristian 1973; Boronson & Oke 1982, 1984). The properties of this host galaxy, the existence of a second bright compact component, 3C 48A, 1″ northeast of the QSO (Stockton & Ridgeway 1991; Zuther et al. 2004), the tail-like extension to the north-east (Canalizo & Stockton 2000), and the richness of 3C 48 in molecular gas (Scoville et al. 1993; Wink et al. 1997, hereafter W97) have all been used as arguments that the activity in 3C 48 is due to a recent merger.

An uncertainty in the merger picture for 3C 48 has been the unknown nature of 3C 48A. Although Zuther et al. (2004) recently detected 3C 48A in the near-IR, suggesting it may be a second nuclear bulge, those authors noted that 3C 48A may simply result from the interaction of the radio jet with the surrounding interstellar medium in the host galaxy (see also Chatzichristou et al. 1999). Our new CO results in this paper strengthen the idea that 3C 48A is indeed a second nuclear bulge, surrounded by a massive circumnuclear disk of molecular gas.

Because two tidal tails are often seen in major mergers, the absence of a tidal counter-tail in 3C 48 has been another mystery in the merger scenario, but Scharwächter et al. (2004) recently proposed a simple solution for the missing tidal counter-tail. Whereas previous papers suggested that the tail extends from southeast to southwest (Canalizo & Stockton 2000), or confused a background galaxy with the counter-tail (Boyce et al. 1999; Canalizo & Stockton 2000), Scharwächter et al. suggest that the counter-tail is in front of the main body of the 3C 48 host galaxy, running from southwest to north-east. They assume a similar configuration as in the Antennae galaxies but viewed from a different angle (as in the diagrams of Toomre & Toomre 1972), and supported their picture with multi-particle simulations that agree better with the observed stellar kinematics than in previous scenarios.

The information on molecular gas in 3C 48 began with Scoville et al. (1993)'s detection of CO(1–0) with the Caltech interferometer. Wink et al. (1997) then confirmed Scoville et al.'s CO results with the IRAM Interferometer. Both groups found a large mass of molecular gas, a few times 10^{10} $M_{\odot}$. Because the molecular gas plays a major role in forming new stars and fueling a black hole, further study of the molecular gas in 3C 48 may help us to understand the many steps leading to the intense nuclear activity of quasars.

In this paper, we present new interferometer observations of the CO(1–0) line and the 3.5 and 1.2 mm continuum emission in 3C 48. To increase the sensitivity, the data were combined with the earlier measurements by Wink et al. (1997). The combined data set is about twice as sensitive as the W97 data. In this paper, Sect. 2 gives details of the new observations. Section 3

Table 1. Continuum data at 3.5 mm and 1.2 mm from all available data sets.

Observing date	RA[a] J2000 (hh:mm:ss)	Dec[a] J2000 (dd:mm:ss)	Continuum flux density[c] 3.5 mm (mJy)	1.2 mm (mJy)	3.5 mm beam maj., min., PA (″, ″, °)	Reference
Observations:						
1992	–	–	266	–	10.5″ × 8.6″	Scoville et al. (1993)
1995-W97	–	–	307 ± 30	–	4.3″ × 1.8″, 34°	Wink et al. (1997)
1995-new[b]	01:37:41.29	33:09:35.4	303 ± 30	–	4.0″ × 2.0″, 38°	this paper
2003	01:37:41.30	33:09:35.5	270 ± 27	82 ± 8[d]	2.3″ × 2.0″, 44°	this paper
Three-Component Model[e]:						
"QSO"			–	36 ± 8		
"Jet"			–	15 ± 4		
"3C 48A"			–	25 ± 7		

[a] Centroid of the 3.5 mm continuum emission.
[b] Our re-reduction of W97's data.
[c] Flux errors include 10% systematic errors.
[d] Total flux of all components, beam at 1.2 mm: 0.9″ × 0.7″ at PA 15°.
[e] Fluxes derived by fitting 3 Gaussian components in the sky plane at 1.2 mm (see Fig. 4).

presents the results of the combined data sets for the mm continuum and the CO emission. In Sect. 4, we discuss the estimate of the molecular gas mass. In Sect. 5, we compare 3C 48 with two other mergers, the "Antennae" galaxies and Arp 220, and summarize our results in Sect. 6.

2. Observations

We used two independent data sets of the CO(1–0) emission in 3C 48, observed with the IRAM interferometer on Plateau de Bure, France. The first was taken by Wink et al. (1997) between November 1994 and February 1995 in the interferometer's B and C configurations with 3 antennas. We re-reduced the data from W97 (see below), and merged them for the analysis of the CO emission with our second data set, observed between December 2002 and March 2003 in the A and C configurations with 6 antennas. Following W97, we chose 3C 84 and 3C 111 as amplitude and phase calibrators. 3C 84 was also used to calibrate the RF bandpass. The receiver at 3.5 mm was tuned to 84.17 GHz, the frequency of ^{12}CO(1–0) at $z = 0.3695$, and the receiver at 1.2 mm to 241.39 GHz, the frequency of ^{13}CO(3–2) at $z = 0.3695$. We used a total bandwidth of 580 MHz at 3.5 mm and 2×580 MHz (DSB) at 1.2 mm with a frequency resolution of 1.25 MHz. The phase center was adopted from W97, i.e. set to $01^{h}37^{m}41.3^{s}$, +33°09′35.0″ (J2000). This is identical with the radio position of the QSO (e.g., Feng et al. 2005). The total on-source integration time was ∼6.5 h. Although the 1.2 mm receiver was tuned to the redshifted frequency of ^{13}CO(3–2), no 1.2 mm line signal was detected to a flux limit of 3.4 Jy km s^{-1} over the same velocity range of −220 to +160 km s^{-1} where the CO(1–0) is observed. The 1.2 mm observations were therefore used for the 3C 48 continuum data.

The most critical point in merging data sets from different epochs with each other is the flux calibration. However, for our re-reduction of W97's data we adopted the flux calibration described in W97 resulting in an accuracy of ∼10%. Except slightly different beam sizes which can be traced back to slightly different data flagging, our re-reduction of W97's data is consistent with the one done by W97. For our new data, we relied on the flux monitoring which is regularly done at the IRAM PdBI giving an accuracy of ∼10% at 3.5 mm. In summary, this would yield an uncertainty of $\lesssim$20% of the merged data in the worst case. As will be discussed in Sects. 3.1.1 and 3.2.1, the fluxes and positions derived for the CO and continuum emission in the two data sets agree well with each other within ∼10% justifying thus a merging.

3. The data

3.1. Continuum

The strong mm continuum emission by itself shows the intense nuclear activity in 3C 48. The mm continuum is from synchrotron radiation, not dust.

3.1.1. The 3.5 mm continuum

We independently measured the 3.5 mm continuum fluxes from both our re-reduction of the 1995 data and our new 2003 data by averaging all channels more than ±380 km s^{-1} from the CO line. The flux from our re-reduction of the 1995 data agrees with that from W97, while the flux from the 2003 data is 10% lower, which is within the systematic errors in the flux calibration, but may just be a real effect, possibly due to intrinsic variability of 3C 48 (Table 1).

The position obtained from our mm-observations is 0.4″ north of that given by 13 and 3.5 cm VLBI measurements (Ma et al. 1998). This difference is probably due to the VLBI observations picking out the low-flux, milliarcsecond-scale hot spot near the quasar (see the maps by Wilkinson et al. 1991 and by Feng et al. 2005), while the mm interferometer sees mainly the high-flux, arcsecond-scale jet. While this position difference is about twice the astrometric uncertainty limit of the IRAM interferometer, a comparison with the recent NIR

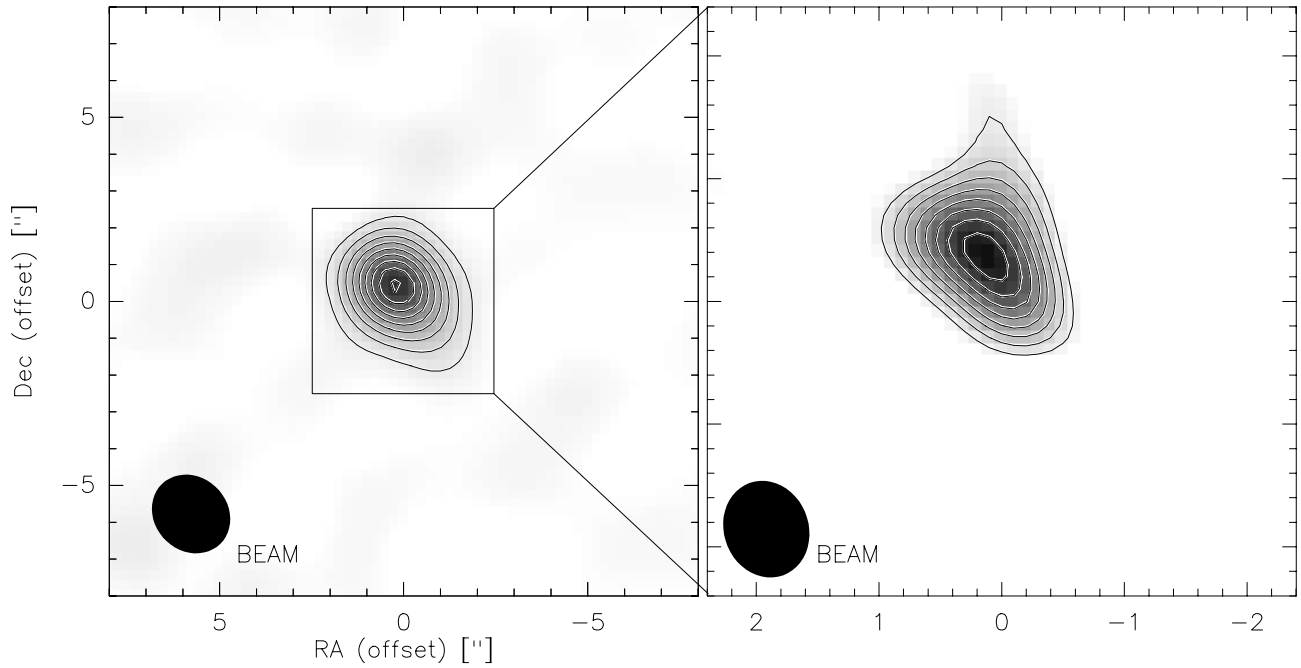

Fig. 1. Continuum maps at 3.5 mm (*left*) and 1.2 mm (*right*) made with the IRAM interferometer in 2003, shown as both contours and greyscale. Contour levels at 3.5 mm are 0.025 to 0.23 by 0.025 Jy/beam (20σ). Contour levels at 1.2 mm are 0.01 Jy/beam (5σ) to 0.044 Jy/beam by 0.004 Jy/beam (2σ). Both maps were made with uniform weighting. Beams are 2.3″ × 2.0″ at PA = 44° at 3.5 mm and 0.8″ × 0.7″ at PA = 20° at 1.2 mm.

images of 3C 48-QSO and 3C 48A nevertheless suggests that the mm continuum may be located between the two NIR features (Fig. 2).

The continuum emission is slightly extended in the 2″ beam (Fig. 1) at 3.5 mm. The two nuclear components are not resolved but the peak flux of 230 mJy/beam is lower than the integrated flux density of 270 mJy, so the continuum is not a single point source. This is also evident from the cm-radio maps and spectra published by Feng et al. 2005. Most of the (cm-)radio continuum flux comes from the radio jet and/or the northeast component 3C 48A. The continuum flux at 3.5 mm falls on the steep spectrum (with $S_\nu \propto \nu^{-1}$) observed at cm wavelengths (Fig. 3 and Meisenheimer et al. 2001). The continuum emission at 3.5 mm is thus still dominated by the jet's synchrotron radiation, not thermal dust emission.

3.1.2. The 1.2 mm continuum

The 1.2 mm continuum was observed only in the 2003 data set (Fig. 1). Because we found no line emission at 1.2 mm, we averaged the continuum over the entire bandwidth of 2×580 MHz (DSB). The continuum was detected with a SNR of ∼25, well-centered on the 3.5 mm position. The emission appears extended to the northeast, toward the near-IR component 3C 48A and toward the north of the radio jet (Fig. 2). These extensions are similar to those on the 18 cm MERLIN map (Akujor et al. 1994). This motivated us to fit three Gaussian components (3C 48A-QSO, 3C 48A, and the jet) to our 1.2 mm map (Fig. 4), both to explain the unusual shape, and to estimate fluxes for each of the possible Gaussian components to ∼4σ-accuracy (Table 1). Extrapolating the cm continuum fluxes to 1.2 mm

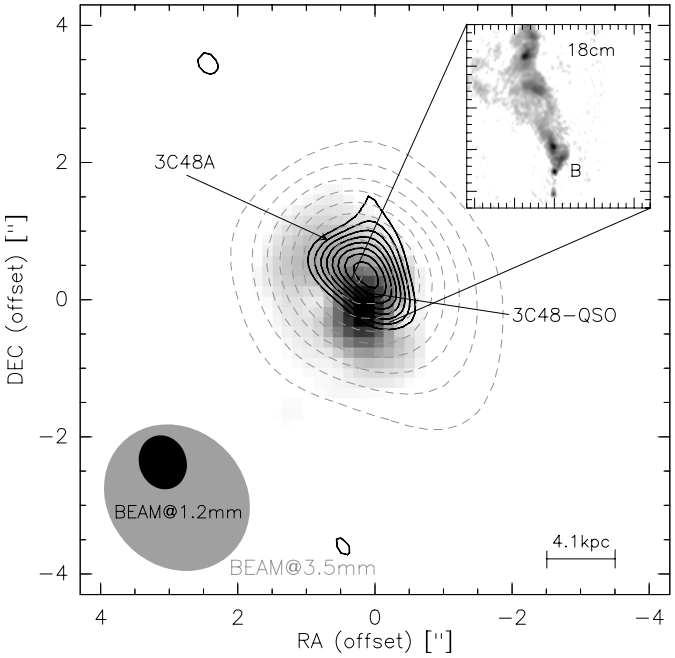

Fig. 2. Contours of the 3.5 mm (*grey dashed lines*) and 1.2 mm (*black solid lines*) continuum observed in 2003. The contours are the same as in Fig. 1, and are superposed on the greyscale NIR-image (Zuther et al. 2004) with the QSO nucleus subtracted (its position agrees with the radio QSO position and is thus located at zero in our maps). The radio jet at 18 cm is plotted in the small box (*upper right*; from Wilkinson et al. 1991; tickmarks correspond to 0.1″). B denotes the position of the QSO.

with the steep spectral index of $\alpha = -1$ ($S_\nu \propto \nu^\alpha$; Fig. 3) yields a flux close to the measured flux of the QSO and jet.

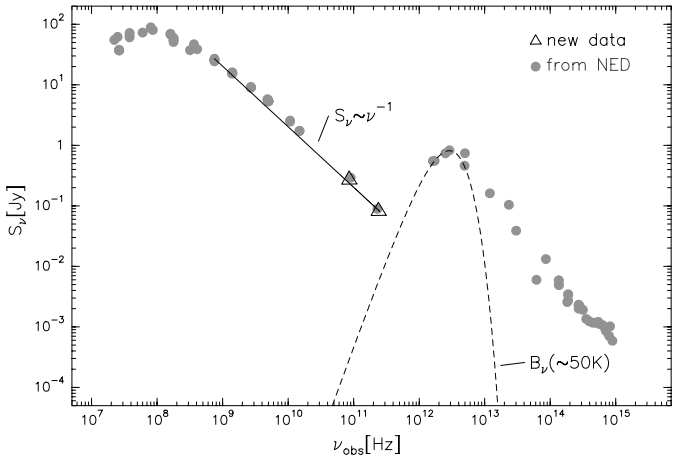

Fig. 3. Flux density spectrum of 3C 48. Grey points are from the NASA/IPAC Extragalactic Database (NED). The triangles at 3.5 mm and 1.2 mm are from our new data, and are the total flux of our continuum fit components. The solid line is a power-law fit to the cm-radio synchrotron emission, and the dashed curve in the infrared (2–10 THz) is a model spectrum for a rest-frame dust temperature of 50 K, a dust $\tau = 1$ at rest-frame 100 μm, and an optically-thin, ν^4 dependence in the mm range.

That is, even at 1.2 mm, the optically thin synchrotron radiation from the jet still predominates over the expected dust flux from the CO source (by more than an order of magnitude; compare Fig. 3).

The Gaussian-fit estimate of the 1.2 mm continuum from 3C 48A, is probably also dominated by non-thermal emission. The 18 cm map by Feng et al. (2005) definitely shows non-thermal emission at the position of 3C 48A and the radio fluxes together with the 1.2 mm estimate obey a power law that is consistent with synchrotron emission. However, the finding of Zuther et al. (2004) that 3C 48A is highly reddened by dust suggests that 3C 48A is also a source of dust emission. This might be still negligible at 1.2 mm but becomes important at submm wavelengths.

The 3.5 mm continuum probably also has contributions from the VLBI hot spot near the quasar, 3C 48A, and the jet. Although our 3.5 mm beam is too large to discriminate among these components, it seems quite likely that at least the hot spot *B* near the base of the jet (Wilkinson et al. 1991 and Fig. 2) and the extended jet itself contribute to the 3.5 mm flux. To estimate these contributions, we adopted the 1.2 mm model for the 3.5 mm data, for a spectral index of −1 between 3.5 and 1.2 mm and smoothed it to the beam at 3.5 mm. Figure 5 suggests that our 1.2 mm model also holds for the 3.5 mm data. Obviously, higher-resolution observations are needed at 3.5 mm and 1.2 mm to confirm the three continuum components we propose for 3C 48.

3.2. Line emission

3.2.1. ^{12}CO(1–0)

To allow for possible source variability, the continuum was subtracted in the uv-plane separately for the 1995 and 2003 data

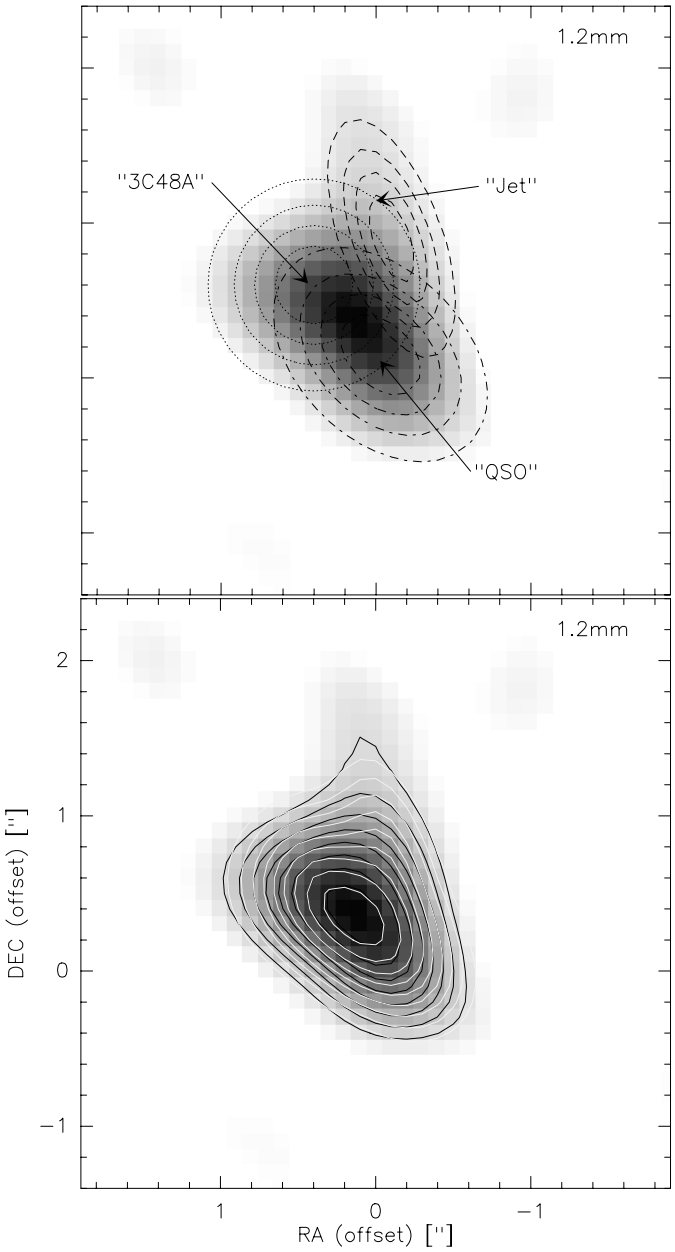

Fig. 4. *Upper panel:* contours of a triple-Gaussian model: "QSO" (*dotted/dashed lines*), "jet" (*dashed lines*), and "3C 48A" (*dotted lines*). Contours are from 20 to 100% in steps of 20% of the peak fluxes of each component. *Lower panel:* the sum of the model components (*white solid contours*), compared with the observed 1.2 mm continuum (*grey scale and black solid contours*); data and model contours are as in Fig. 2. Data are taken from the 2003 data set only.

sets. The line peak fluxes in the W97 data and our new data agree within the errors and with the value found by Scoville et al. (1993). The measured linewidths and positions also agree within the errors among the different data sets (see Table 2). Thus, the final (continuum-free) channel maps of the 1995 and 2003 data were finally merged.

Figure 6 shows the merged maps of the CO(1–0) line in 11 MHz channels. CO(1–0) emission is detected with a SNR of 4 to 5 in individual channels from −200 km s^{-1} to +120 km s^{-1}. A single Gaussian fit to the spectrum (Fig. 7) at

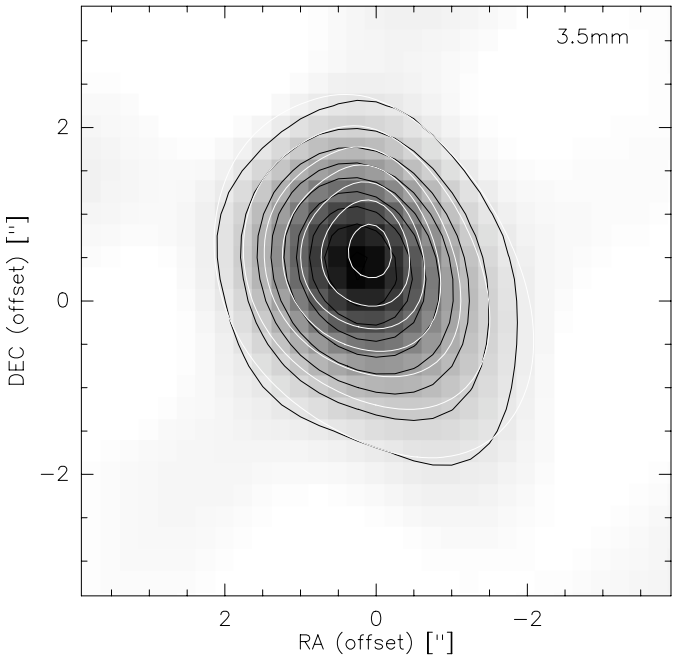

Fig. 5. Continuum emission at 3.5 mm (*grey scale and black solid contours*; 2003 data only) overlaid with contours of a three Gaussian component model taken from 1mm with corrected fluxes and smoothed to the 3.5 mm beam (*white solid lines*). Contours of solid lines (*lower panel*) for model and data as in Fig. 2.

the centroid of the CO(1–0) emission yields the line parameters given in Table 2. We then subtracted the fit profile, and found that the residual spectrum had an rms noise of 1.9 mJy, twice as high as the measured rms noise of ∼0.9 mJy at off-source positions. The single Gaussian fit is thus probably too simple to account for the observed line shape, but a better signal-to-noise ratio would be needed for fitting multiple line components.

The integrated emission over the whole velocity range (from −220 to 160 km s^{-1}) is shown in Fig. 8. The centroid of the total CO(1–0) emission is located between the QSO and 3C 48A. The emission nicely covers the QSO and 3C 48A and we find two extensions, one to the north and one to the southwest, neither of which are aligned with the major axis of the beam. The position-velocity diagrams along the two cuts[1] shown in Figs. 8 and 10 suggest three different velocity components. A velocity gradient is visible over velocities −120 to +80 km s^{-1}. Two further components at −200 km s^{-1}and +120 km s^{-1} appear to be unrelated to the "inner" velocity gradient. Motivated by these diagrams, we made three different integrated intensity maps over the respective velocity ranges (Fig. 10). The positions of the CO components relative to the infrared components led us to label the main CO feature, at velocities −120 km s^{-1} to +80 km s^{-1}, as "3C 48A-CO", and the other two features as "QSO-red" (+120 km s^{-1}) and "QSO-blue" (−200 km s^{-1}). The 3C 48A-CO component is centered close to the 3C 48A-IR source, while the QSO-red-CO and QSO-blue-CO features are roughly centered on the QSO-IR source, close to the QSO VLBI position. All three CO components appear slightly extended in the interferometer beam, but the signal-to-noise is not high enough to derive source diameters.

[1] The cut at PA = 33° (with respect to QSO-red) was choosen to run along the velocity gradient seen in Fig. 11 and to hit still 3C 48A and QSO-red (Fig. 10), while the cut at PA = 116° should go through QSO-red and QSO-blue (Fig. 10). See next subsections for more details.

Table 2. CO(1–0) positions, peak fluxes, and linewidths.

Epoch	RA offset[b] (″)	Dec offset[b] (″)	CO(1–0) peak flux (mJy/beam)	Linewidth *FWHM* (km s^{-1})
1992[a]	–	–	∼7	∼250
W97	–	–	9 ± 2	270 ± 20
1995[c]	−0.5 ± 0.6	0.0 ± 0.6	9 ± 2	240 ± 40
2003	0.5 ± 0.4	0.0 ± 0.4	6 ± 2	330 ± 50
2003+1995	0.3 ± 0.3	0.0 ± 0.3	6 ± 1	320 ± 30

[a] From Scoville et al. (1993).
[b] Relative to 01^{h}37^{m}41.30^{s}, +33°09′35″ (J2000).
[c] From our re-reduction of the W97 data.

3.2.2. The 3C 48A-CO velocity gradient

At velocities corresponding to 3C 48A-CO (−120 km s^{-1} to +80 km s^{-1}), the CO centroid moves from south-west (positive velocities) to north-east (negative velocities) in Fig. 6. Such a variation in position was already suggested by W97 but their signal-to-noise ratio was poor. In our new 2003 data, this shift is highly significant. The velocity gradient is clearly visible in the isovelocity map (Fig. 11, *right*) and in the pv-diagram (Fig. 9).

3.2.3. QSO-blue and QSO-red CO components

In Figs. 6, 9, and 10, another two compact CO features are seen at −180 km s^{-1} and at +120 km s^{-1}, that we label as QSO-blue (at 5σ) and QSO-red (at 6σ). In both the integrated intensity map (Fig. 10), and in the p-v diagram (Fig. 9) along the cut in the upper and lower panels of Fig. 10, the centroids of these two components differ by 0.5″. Within the 0.3″ positional uncertainties due to the low signal-to-noise ratio, however, the two features roughly coincide with each other and with the QSO. We think these two components may arise in a circumnuclear disk of molecular gas around the QSO.

4. Gas mass and dynamical mass in 3C 48

Table 3 lists the gas masses (H_2 plus helium) that we estimate from the CO(1–0) luminosities, using the mean conversion factor of $0.8\,M_\odot\,(\mathrm{K\ km\ s^{-1}\ pc^2})^{-1}$ obtained by Downes & Solomon (1998) by kinematic/radiative-transfer modeling of the molecular gas in the circumnuclear regions of Ultra-Luminous InfraRed Galaxies (ULIRGs). This value is a factor of six lower than the value that would hold in self-gravitating molecular clouds in spiral arms of the Milky Way, and is relatively insensitive to assumed [CO]/[H_2] abundances, because the CO is opaque. As a check, one may estimate a *lower* limit on the molecular gas mass, by assuming the CO is

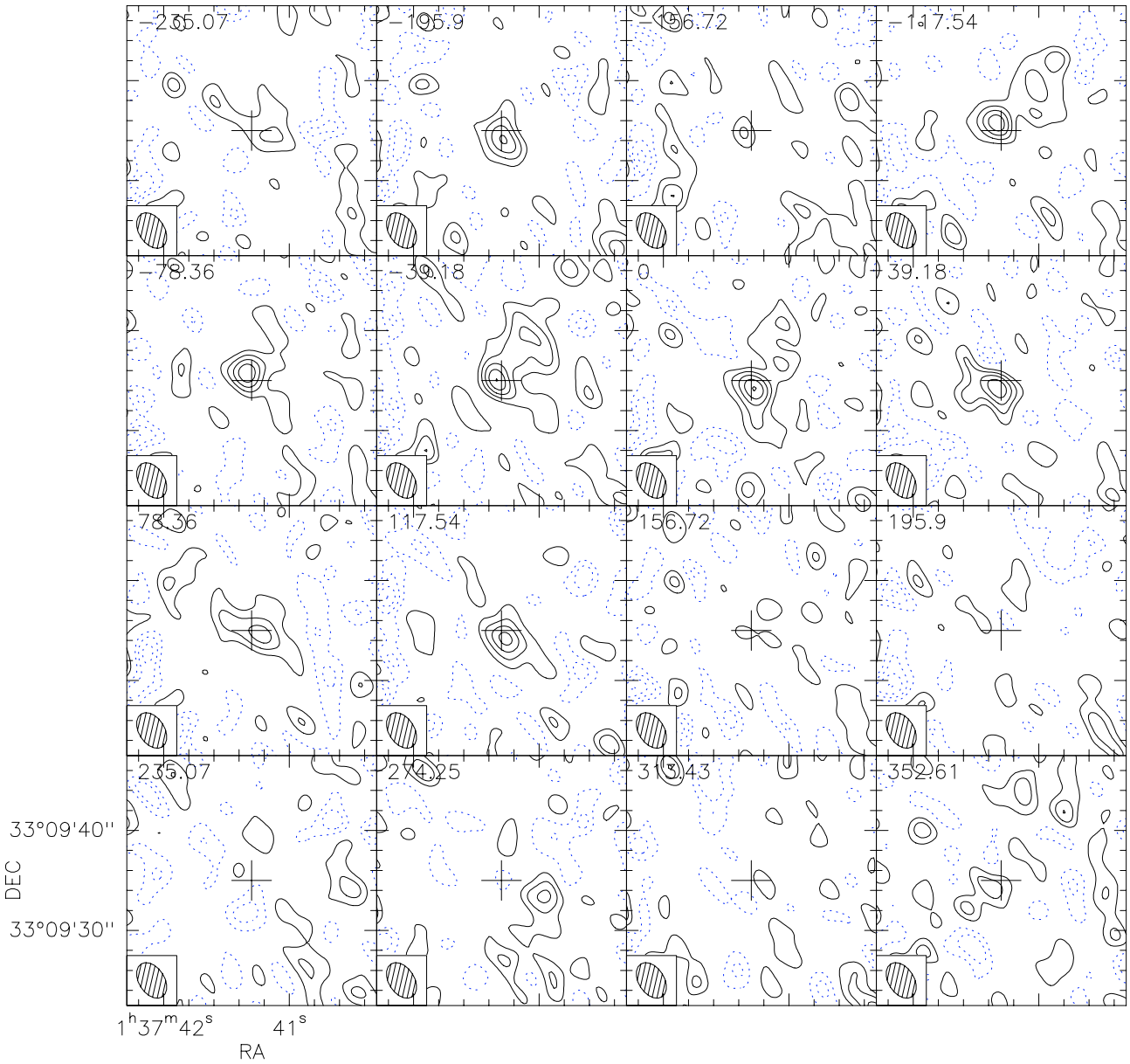

Fig. 6. CO(1–0) channel maps from the merged 1995+2003 data. Positive and negative contours are in steps of 1.2 mJy beam^{-1} (1σ), up to a maximum of 6.0 mJy beam^{-1}. The natural weighted beam is 3.6″ × 2.5″ at PA = 32°. The cross in the maps denotes the phase center (Sect. 2).

optically thin (Solomon et al. 1997). This method yields a lower limit to the (total) 3C 48 gas mass of $>8 \times 10^9\,M_\odot$. An independent estimate of the gas mass can be made from the optically thin dust flux. For a dust flux density of 0.55 Jy at $\nu_{\rm obs}$ = 1.62 THz (Meisenheimer et al. 2001) and a rest-frame dust temperature $T_{\rm d}$ = 50 K, as in Fig. 3, we obtain a dust mass of $M_{\rm dust} \simeq 1.6 \times 10^8\,M_\odot$. For a gas-to-dust mass ratio of 150, the gas mass would be $M_{\rm gas} \sim 2 \times 10^{10}\,M_\odot$, of the same order as the molecular gas mass estimate from the CO luminosity.

Without size measurements, one cannot obtain reliable values for the dynamical mass (gas plus stars) within the CO-emitting regions. Representative estimates of RV^2/G would be $3.2 \times 10^{10}\,M_\odot$ for an 0.5″-diameter (1.3 kpc radius) circumnuclear disk rotating at 330 km s^{-1} around the 3C 48 quasar, or $6.4 \times 10^{10}\,M_\odot$ for the 3C 48A and 3C 48 nuclei, if their true separation is 5 kpc (1″), and they are orbiting their center of mass at a radius of 2.5 kpc at a velocity of 330 km s^{-1} (the CO linewidth in Table 2). The latter dynamical mass estimate is close to the estimate of the gas mass, but could easily be much higher if the true distance is greater than the projected separation of 3C 48 and 3C 48A on the sky, and/or if the relative velocity of the merger nuclei is greater than 330 km s^{-1}. Thus, the estimate of the dynamical mass should be taken as lower limit.

5. 3C 48 and other sources where CO has been observed in two merger nuclei

In the scenario of Sanders et al. (1988), galaxy interactions and mergers trigger the formation of ULIRGs, which evolve to turn on the activity of the massive black holes at the centers of quasars and radio galaxies. With our new CO evidence for

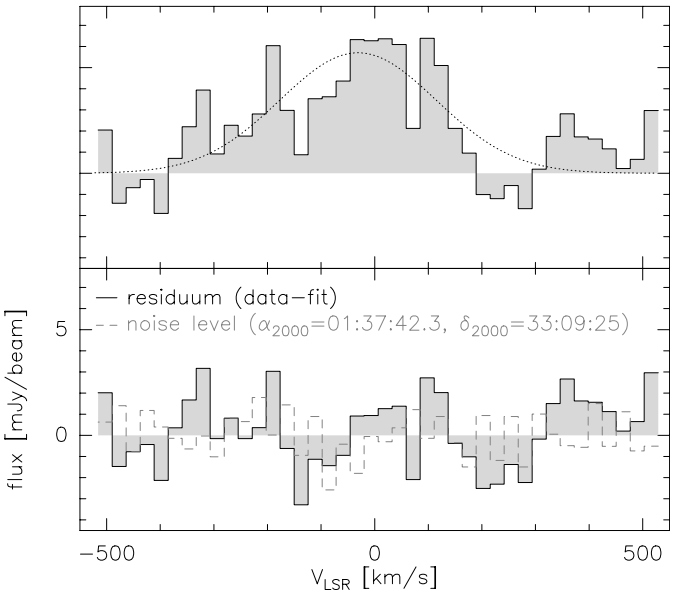

Fig. 7. *Upper panel:* spectrum at the CO(1–0) centroid in 3C 48 taken from the merged 1995 and 2003 data set (solid histogram), with a Gaussian fit to the data. *Lower panel:* residual spectrum after subtracting the fit from the data (dotted line). The dashed histogram is a spectrum taken at an off-source position with no CO emission, where the rms noise is 0.9 mJy. The velocity resolution is 26 km s^{-1}.

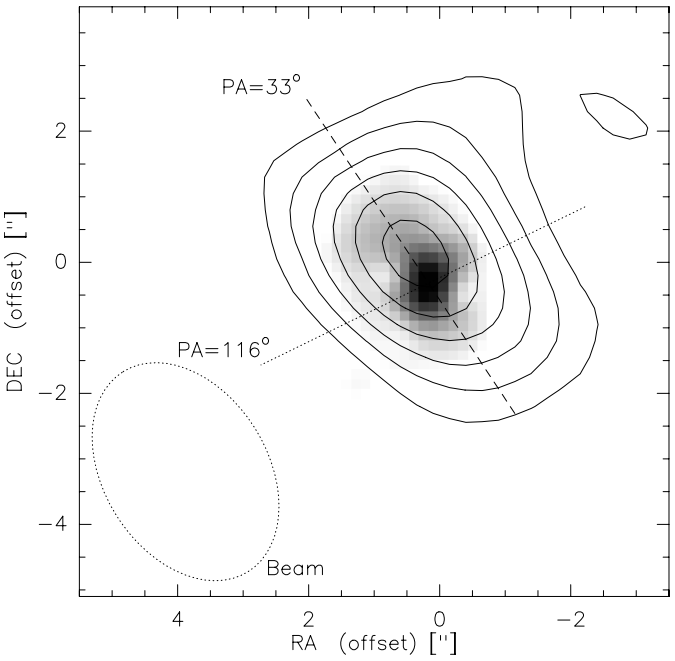

Fig. 8. Integrated CO(1–0) emission of 3C 48 (from −220 km s^{-1} to 160 km s^{-1}; merged 1995 and 2003 data). The synthesized beam is indicated in the lower left (*dotted ellipse*). The *dashed* and *dotted* lines shows the cuts along which the position-velocity diagrams were taken. Contour levels are from (3σ=)0.6 to 1.6 Jy beam^{-1} km s^{-1} by 0.2 Jy beam^{-1} km s^{-1}. Beam: 3.6″ × 2.5″ at PA = 32°. The CO map is superposed on the NIR image of Zuther et al. (2004) (*grey scale*).

two circumnuclear molecular disks, 3C 48 now joins a growing list of powerful AGNs where CO is detected in the merger partners. At low redshifts these include the sample of quasars

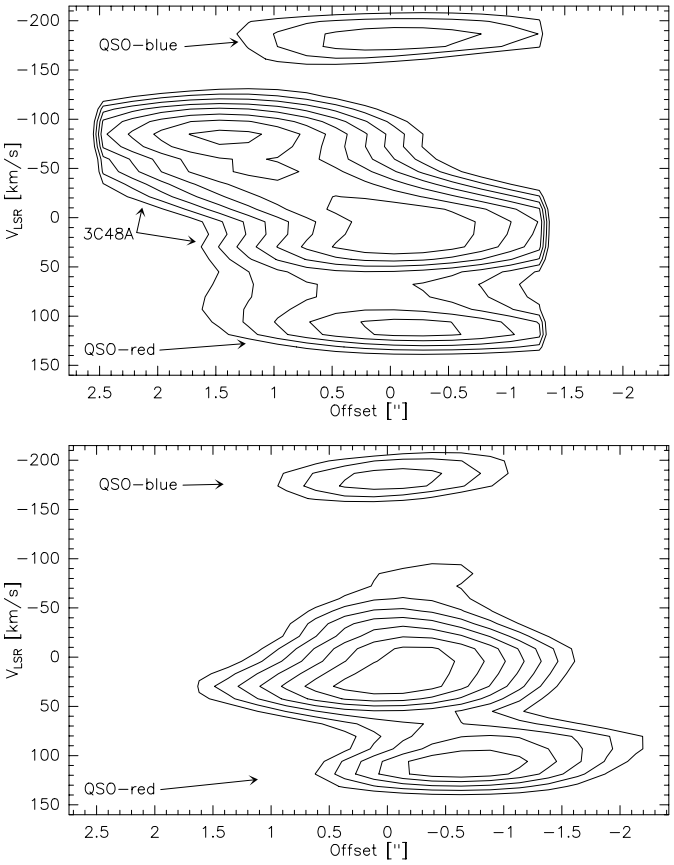

Fig. 9. CO(1–0) position-velocity diagram along the cuts indicated by the dashed lines in Figs. 8 and 10 (merged 1995 and 2003 data set). Contours are from 35% in steps of 5% from the peak. *Upper panel:* the p-v cut from northeast to southwest, shown in Fig. 8 and in the middle panel of Fig. 10. *Lower panel:* the p-v cut from southeast to northwest, shown in Fig. 8 and in the upper and lower panels in Fig. 10. The offsets are relative to the position of the CO-QSO-blue component.

and ULIRGs observed in CO by Evans et al. (2001, 2002), some of which have double nuclei. At high redshifts, prominent examples are the two CO systems detected in the powerful radio galaxy 4C 41.17 (De Breuck et al. 2005), the two CO systems in the radio galaxy 4C 60.07 (Papadopoulos et al. 2000; Greve et al. 2004), the double CO sources in the quasars BRI 1202-0725 and BRI 1335-0417 (e.g., Carilli et al. 2002), the two CO nuclei in the $z = 6.4$ quasar J1148+52 (Walter et al. 2004) and the two optical/IR objects L1 and L2 in the quasar SMMJ02399+0256 (Ivison et al. 1998). For this last quasar, we think the two CO velocity peaks, first detected by Frayer et al. (1998), correspond to the two circumnuclear disks of the merger, rather than a single large disk as proposed by Genzel et al. (2003).

Because most luminous, low-redshift QSOs appear to be in gas-rich host galaxies (Scoville et al. 2003), it is worth reviewing the two best-known nearby mergers of gas-rich galaxies, and their effects on the molecular gas – Arp 220 at a distance of 75 Mpc, and the "Antennae" galaxies (NGC 4038/39) at a distance of 18 Mpc. Because they have been so well-studied, the tidal tails of the Antennae galaxies were used by Scharwächter et al. (2004) to simulate possible tidal tails, viewed from

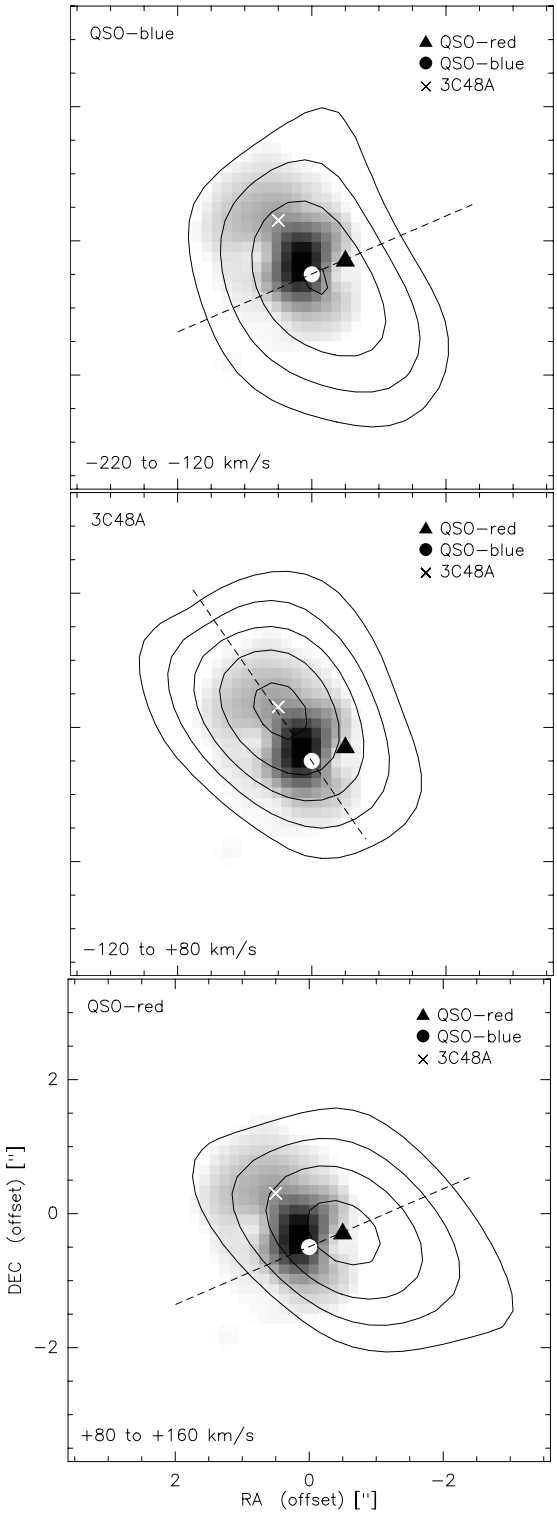

Fig. 10. CO(1–0) integrated over the following ranges (merged 1995 and 2003 data set): *Upper:* QSO-blue, from −220 to −120 km s^{-1}; contours run from (2σ=)0.08 to 0.2 Jy beam^{-1} km s^{-1} in steps of 1σ. *Middle:* 3C 48A, from −120 to 80 km s^{-1}; contours run from (3σ=)0.42 to 0.98 Jy beam^{-1} km s^{-1} in steps of 1σ. *Lower:* QSO-red, from 80 to 160 km s^{-1}; contours run from (3σ=)0.15 to 0.3 Jy beam^{-1} km s^{-1} in steps of 1σ. Dashed lines show the cuts on which the pv-diagrams were made. The CO beam is 3.6″ × 2.5″. All the CO maps are superposed on the NIR image of Zuther et al. (2004) (*grey scale*).

a different angle, in 3C 48. The optical morphology (e.g. Whitmore et al. 1999), shows the Antennae galaxies to be an early-stage merger of two gas-rich spiral galaxies. Gao et al. (2001) derive a molecular gas mass of ($\sim 1.5 \times 10^{10}$ $M_\odot$), extended over both galaxies. There is a large amount of molecular gas of $\sim 4 \times 10^9$ $M_\odot$ in the overlapping region of the two galaxies (Zhu et al. 2003). The CO, the mid- and far-infrared, and the submm- and cm-radio continuum all peak in the region between the two merging disks. The large IR luminosity of $\sim 10^{11}$ $L_\odot$ puts the Antennae galaxies in the LIRG class (Sanders & Mirabel 1996). From long-wavelength studies (e.g. Hummel & van der Hulst 1986; Mirabel et al. 1998; Haas et al. 2000; Neff & Ulvestad 2000), it is clear the IR luminosity of the Antennae galaxies is due to system-wide star formation, not an AGN. The two nuclei ∼7 kpc projected separation of the two nuclei is about the same as that of 3C 48 and 3C 48A.

Arp 220 has a high molecular gas content of $\sim 10^{10}$ $M_\odot$ within the central kiloparsec (Scoville et al. 1986). It also contains two nuclear components with a projected separation of 300 pc, and an extended tidal tail that led to the hypothesis of an ongoing merger (e.g., Norris 1985; Graham et al. 1990). The huge IR luminosity ($L_{8-1000\,\mu\mathrm{m}} = 1.4 \times 10^{12}$ $L_\odot$) puts it in the ULIRG class (Soifer et al. 1987). Scoville et al. (1998) report on a high near-IR obscuration of one of the two nuclei, as is the case in 3C 48A (Zuther et al. 2004). Besides a large molecular gas disk ($r \sim 1$ kpc) rotating around the dynamical center of the system, high resolution (∼0.5″) observations of the CO emission unveil nuclear disks ($r \sim 100$ pc) around both nuclei (Downes & Solomon 1998). These two nuclear disks appear to rotate orthogonally with respect to each other and have molecular gas masses of 10^9 $M_\odot$ and dynamical masses of $\gtrsim 2 \times 10^9$ $M_\odot$ (Sakamoto et al. 1999). Eckart & Downes (2001) showed that the Arp 220 CO kinematics may also be interpreted as a single, warped disk. Except for the scale, the overall situation in 3C 48 resembles that in Arp 220. Our CO data in this paper suggest that there are also two rotating, molecular gas disks in 3C 48. The main difference is that 3C 48 is a powerful quasar, while no obvious AGN has been identified in Arp 220.

6. Summary and conclusions

- 1) Our new CO(1–0) results show that the main part of the emission – the central part of the CO line actually comes from 3C 48A, not the quasar. The higher sensitivity of the new CO data shows a clear velocity gradient across 3C 48A, indicating rotation of a disk of molecular gas at 3C 48A, with an extension toward the north and southwest. This CO concentration is the strongest argument supporting the idea that 3C 48A is a second nucleus.
- 2) The data clearly indicate two different dynamical systems in the molecular gas: the extended disk toward 3C 48A, and a second, independent gas reservoir to the southwest, around the QSO itself.
- 3) The total molecular gas mass of a few times 10^{10} $M_\odot$ is typical of the circumnuclear disks in advanced-merger ULIRGs.
- 4) The 1.2 mm nonthermal continuum was mapped for the first time at resolution of ∼0.8″, and observed to be

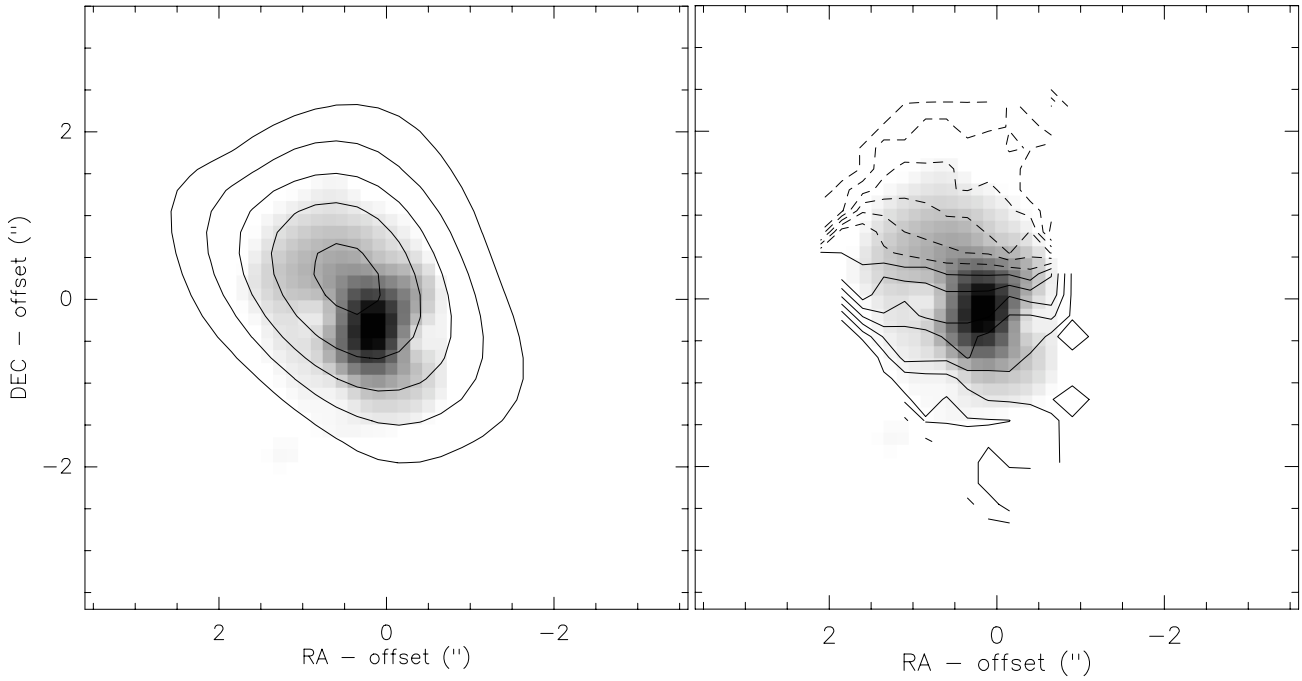

Fig. 11. *Left:* 3C 48 integrated CO(1–0) emission from −120 to +80 km s^{-1}. Contours are 0.2 to 0.8 Jy beam^{-1} km s^{-1} by 0.1 Jy beam^{-1} km s^{-1}. The CO beam is 3.5″ × 2.6″. *Right:* CO isovelocity map. Velocity contours run from −95 to −45 km s^{-1} (*dashed*) and −35 to 25 km s^{-1} (*solid*) in steps of 10 km s^{-1}. Both CO maps are superposed on the NIR image of Zuther et al. (2004) (*grey scale*). Data are taken from the merged 1995 and 2003 data sets.

Table 3. CO(1–0) luminosities and gas masses[a].

CO source component	Integrated CO flux (Jy km s^{-1})	Luminosity $L'_{\rm CO}$ (K km s^{-1} pc^2)	Gas mass M(H$_2$+He) (10^{10} $M_\odot$)
3C 48A	1.2 ± 0.2	8×10^9	0.6 (3.6)[b]
QSO-blue	0.3 ± 0.1	2×10^9	0.2 (0.9)[b]
QSO-red	0.3 ± 0.1	2×10^9	0.2 (0.9)[b]
Total	1.9 ± 0.2	12×10^9	1.0 (5.6)[b]

[a] CO luminosities and gas masses are for H_0 = 71 km s^{-1} Mpc^{-1}, $\Omega_{\rm m}$ = 0.27, and Ω_Λ = 0.73, which yield an angular diameter distance of 3C 48 of 1.044 Gpc. 1″ corresponds to 5.06 kpc.

[b] The gas masses were derived using 0.8 (K km s^{-1} pc^2)$^{-1}$ (see text), while the values in brackets are estimated via the standard conversion factor of 4.6 (K km s^{-1} pc^2)$^{-1}$.

extended. At 1.2 mm, the continuum is clearly elongated towards the second NIR nuclear component 3C 48A and the radio jet. These extensions are consistent with that on the 18 cm MERLIN map (Akujor et al. 1994). The 3.5 mm continuum data also suggest extended emission towards 3C 48A.

– 5) Model fits to the 1.2 mm continuum suggests three distinct components: one at the 3C 48 QSO to the southwest, one along the extended jet to the north and a third one at the position of the candidate second merger nucleus 3C 48A to the north-east. While the 1.2 mm components corresponding to both the QSO hot spot and the radio jet are synchrotron emission, the 3C 48A component may have a partial contribution from thermal dust emission at 1.2 mm. Higher-resolution mm and submm continuum observations (e.g. with the SMA or the upgraded PdBI) are needed to better separate the components and to analyse the contribution of thermal and non-thermal emission.

– 6) In the 1.2 mm continuum, 3C 48A is located to the east of the jet, i.e. does not align with the jet. This shows that the jet does not hit 3C 48A head-on. A possible but still speculative explanation might be that the non-collimated and diffuse jet has been disrupted a first time by the dense circumnuclear disk around the quasar itself, and then diverted a second time, to the north, by the magnetic field pressure associated with 3C 48A (see the 1.66 GHz map by Wilkinson et al. 1991, their Fig. 1).

– 7) 3C 48 joins a growing list of quasars in which *two* merger nuclei have been detected in CO. 3C 48 shows similar properties to these double-CO-nuclei quasars at low and high redshift, and also to the molecular gas in nearby non-quasar mergers like Arp 220 and the Antennae galaxies. All these objects have high molecular gas masses of a few times 10^{10} $M_\odot$, high infrared luminosities and have two components with different projected separations interpreted as two nuclei.

Acknowledgements. We thank T. L. Wilson & S. Guilloteau for kindly providing their earlier data (Wink et al. 1997, W97) and for helpful discussion. Part of this work was supported by the German *Sonderforschungsbereich, SFB,* project number 494. This paper was based on observations with the IRAM Interferometer. IRAM is supported by INSU/CNRS (France), MPG (Germany) and IGN (Spain).

References

Akujor, C. E., Luedke, E., Browne, I. W. A., et al. 1994, A&AS, 105, 247
Boronson, T. A., & Oke, J. B. 1982, Nature, 296, 397
Boronson, T. A., & Oke, J. B. 1984, ApJ, 291, 535
Canalizo, G., & Stockton, A. 2000, ApJ, 528, 201
Carilli, C. L., Kohno, K., Kawabe, R., et al. 2002, AJ, 123, 1838
Chatzichristou, E. T., Vanderriest, Ch., & Jaffe, W. 1999, A&A, 343, 407
De Breuck, C., Downes, D., Neri, R., et al. 2005, A&A, 430, L1
Downes, D., & Solomon, P. M. 1998, ApJ, 507, 615
Eckart, A., & Downes, D. 2001, ApJ, 551, 730
Evans, A. S., Frayer, D. T., Surace, J. A., & Sanders, D. B. 2001, AJ, 121, 3286
Evans, A. S., Mazzarella, J. M., Surace, J. A., & Sanders, D. B. 2002, ApJ, 580, 749
Feng, W. X., An, T., Hong, X. Y., et al. 2005, A&A, 434, 101
Frayer, D., Ivison, R. J., Scoville, N. Z., et al. 1998, ApJ, 506, L7
Gao, Yu, Lo, K. Y., Lee, S.-W., & Lee, T.-H. 2001, ApJ, 548, 172
Genzel, R., Baker, A. J., Tacconi, L. J., et al. 2003, ApJ, 584, 633
Graham, J. R., Matthews, D. P., Neugebauer, G., Soifer, B. T., & Wilson, T. D. 1990, ApJ, 354, L5
Greve, T., Ivison, R., & Papadopoulos, P., 2004, A&A, 419, 99
Haas, M., Klaas, U., Coulson, I., Thommes, E., & Xu, C. 2000, A&A, 356, 83
Hummel, E., & van der Hulst, J. M. 1986, A&A, 155, 151
Ivison, R. J., Smail, I., Le Borgne, J.-F., et al. 1998, MNRAS, 298, 583
Kristian, J. 1973, ApJ, 179, L61
Ma, C., Arias, E. F., Eubanks, T. M., et al. 1998, AJ, 116, 516
Matthews, T. A., Bolton, J. G., Greenstein, J. L., Munch, G., & Sandage, A. R. 1961, Sky and Telescope 21, 148
Meisenheimer, K., Haas, M., Müller, S. A. H., et al. 2001, A&A, 372, 719
Mirabel, I. F., Vigroux, L., Charmandaris, V., et al. 1998, A&A, 333, 1
Neff Susan, G., & Ulvestad James, S. 2000, AJ, 120, 670
Norris, R. P. 1985, MNRAS, 216, 701
Papadopoulos, P., Röttgering, H. J. A., van der Werf, P. P., et al. 2000, ApJ, 528, 626
Sakamoto, K., Scoville, N. Z., Yun, M. S., et al. 1999, ApJ, 514, 68
Sanders, D. B., & Mirabel, I. F. 1996, ARA&A, 34, 749
Scharwächter, J., Eckart, A., Pfalzner, S., et al. 2004, A&A, 414, 497
Scoville, N. Z., Sanders, D. B., Sargent, A. I., et al. 1986, ApJ, 311, L47
Scoville, N. Z., Padin, S., Sanders, D. B., Soifer, B. T., & Yun, M. S. 1993, ApJ, 415, L75
Scoville, N. Z., Evans, A. S., Dinshaw, N., et al. 1998, ApJ, 492, L107
Scoville, N. Z., Frayer, D. T., Schinnerer, E., & Christopher, M. 2003, ApJ, 585, L105
Soifer, B. T., Sander, D. B., Madore, B. F., et al. 1987, ApJ, 320, 238
Solomon, P. M., Downes, D., Radford, S. J. E., & Barrett, J. W. 1997, ApJ, 478, 144
Stockton, A., & Ridgeway, S. E. 1991, AJ, 102, 488
Toomre, A., & Toomre, J. 1972, ApJ, 178, 623
Walter, F., Carilli, C., Bertoldi, F., et al. 2004, ApJ, 615, L17
Whitmore, B. C., Zhang, Q., Leitherer, C., et al. 1999, AJ, 118, 1551
Wilkinson, P. N., Tzioumis, A. K., Benson, J. M., et al. 1991, Nature, 352, 313
Wink, J. E., Guilloteau, S., & Wilson, T. L. 1997, A&A, 322, 427
Yun, M., Reddy, N. A., Scoville, N. Z., et al. 2004, ApJ, 601, 734
Zhu, M., Seaquist, E. R., & Kuno, N. 2004, ApJ, 588, 243
Zuther, J., Eckart, A., Scharwächter, J., Krips, M., & Straubmeier, Ch. 2004, A&A, 414, 919